Synthesis and Evaluation of a Near-Infrared Fluorescent Non-Peptidic Bivalent Integrin $\alpha_v\beta_3$ Antagonist for Cancer Imaging

Feng Li,[†] Jiacheng Liu,[†] Gouri S. Jas,[‡] Jiawei Zhang,[†] Guoting Qin,[†] Jiong Xing,[†] Claudia Cotes,[†] Hong Zhao,[†] Xukui Wang,[†] Laura A. Diaz,[†] Zheng-Zheng Shi,[†] Daniel Y. Lee,[†] King C. P. Li,[†] and Zheng Li*[,†]

Department of Radiology, The Methodist Hospital Research Institute, 6565 Fannin Street, B5-022, Houston, Texas 77030, and Department of Chemistry, Biochemistry, and Institute of Biomedical Studies, Baylor University Sciences Building, Room C322, Baylor University, 101 Bagby Avenue, Waco, Texas 76706. Received July 14, 2009; Revised Manuscript Received December 22, 2009

Computer modeling approaches to identify new inhibitors are essentially a very sophisticated and efficient way to design drugs. In this study, a bivalent nonpeptide intergrin $\alpha_v\beta_3$ antagonist (bivalent IA) has been synthesized on the basis of an in silico rational design approach. A near-infrared (NIR) fluorescent imaging probe has been developed from this bivalent compound. *In vitro* binding assays have shown that the bivalent IA ($IC_{50} = 0.40 \pm 0.11$ nM) exhibited improved integrin $\alpha_v\beta_3$ affinity in comparison with the monovalent IA ($IC_{50} = 22.33 \pm 4.51$ nM), resulting in an over 50-fold improvement in receptor affinity. NIR imaging probe, bivalent-IA-Cy5.5 conjugate, also demonstrated significantly increased binding affinity ($IC_{50} = 0.13 \pm 0.02$ nM). Fluorescence microscopy studies showed integrin-mediated endocytosis of bivalent-IA-Cy5.5 in U87 cells which was effectively blocked by nonfluorescent bivalent IA. We also demonstrated tumor accumulation of this NIR imaging probe in U87 mouse xenografts.

INTRODUCTION

Integrins, a family of cell adhesion molecules, are involved in a wide range of cell−extracellular matrix (ECM) and cell−cell interactions (*1, 2*). Up to now, 18 α and 8 β subunits have been described, which assemble into 24 different receptors (*3*). Among them, integrin $\alpha_v\beta_3$ has been intensively studied due to its important role in tumor angiogenesis and tumor metastasis. It is highly expressed on activated tumor endothelial cells and fast-growing tumor cells but not resting endothelial cells and normal organs; the receptor is therefore suggested as a molecular target for tumor therapy and imaging. Targeting $\alpha_v\beta_3$ by directly inhibiting its function is potentially an effective strategy for cancer treatment. Cyclic arginine-glycine-aspartic acid (RGD) peptide, Vitaxin (MedImmune), and cilengitide (EMD Serono) are currently undergoing clinical trials with melanoma and glioblastoma multiforme patients (*4, 5*). Although a series of monomeric and multivalent RGD peptides have been reported as an anchor for targeting $\alpha_v\beta_3$ in molecular imaging, nonpeptide antagonists were rarely used and few of them have used rational design to construct the optimal multivalent integrin $\alpha_v\beta_3$ ligands (*6, 7*). In this report, we describe the synthesis and evaluation of a bivalent nonpeptide small molecule intergrin $\alpha_v\beta_3$ antagonist based on an in silico rational design approach. A near-infrared (NIR) fluorescent imaging probe has been developed for tumor angiogenesis imaging from this bivalent compound. We demonstrated the improved receptor binding affinity, receptor binding specificity of the bivalent IA, and a promising tumor accumulation of the NIR bivalent IA imaging probe in mouse xenografts.

Previously, we have developed an integrin $\alpha_v\beta_3$ targeting small molecular fluorescent probe derived from a small molecule $\alpha_v\beta_3$ antagonist, 4-[2-(3,4,5,6-tetrahydropyrimidine-2-lamino)-ethyloxy]benzoyl-2-(*S*)-aminoethylsulfonyl-amino-*h*-alanine (Figure 1, IA) (*8*). We have also developed a polymerized liposome-based vascular targeted nanoparticle delivery system using IA as tumor targeting ligand while carrying a payload for simultaneous imaging and therapy (*9*). In this study, we used IA as parent compound and constructed a bivalent ligand with a computer modeling designed linker to enable multivalent ligands to mimic, compete with, or inhibit natural interactions. Linker length and rigidity can affect the multivalent ligand−receptor interaction. In addition, the linkers used should have good physicochemical properties such as high stability and low toxicity. Hence, we chose carbon chain as the backbone of linkers and studied linkers with different lengths by computer simulation to predict the optimal structure for bivalent ligands followed by chemical synthesis and *in vitro* and *in vivo* validation (Figure 1).

Considering more avid binding could improve the tumor targeting properties, we further developed a NIR optical imaging probe based on the bivalent IA for tumor $\alpha_v\beta_3$ integrin imaging. The utilization of NIR probes in cancer imaging strategies has attracted wide attention, because light scattering in tissue decreases with the reciprocal of the fourth power of wavelength and hemoglobin has minimal absorbance and autofluorescence in the NIR window (*10, 11*). NIR imaging technology is relatively inexpensive and absent the biological effects of radioactive probes. In this investigation, our plan was to develop a cyanine dye (Cy5.5) conjugated NIR fluorescent $\alpha_v\beta_3$ bivalent imaging probe (bivalent-IA-Cy5.5) with strong and specific binding. If successful, this imaging probe has great potential for early detection of tumors and micrometastatic lesions.

EXPERIMENTAL PROCEDURES

General. All solvents and reagents were purchased from commercial sources and used without further purification. ^{1}H NMR and ^{13}C NMR were obtained on a Bruker Ultrashield at 300 and 75 MHz, respectively. Chemical shifts were reported in ppm (δ) downfield of tetramethylsilane and coupling constants were given in hertz. The purification of the crude product was carried out on a semipreparative reversed-phase high-perfor-

* Corresponding author. Tel.: +1 713 441 7962. Fax: +1 713 790 3018. E-mail address: zli@tmhs.org.
[†] The Methodist Hospital Research Institute.
[‡] Baylor University.

10.1021/bc900313d
Published on Web 01/26/2010

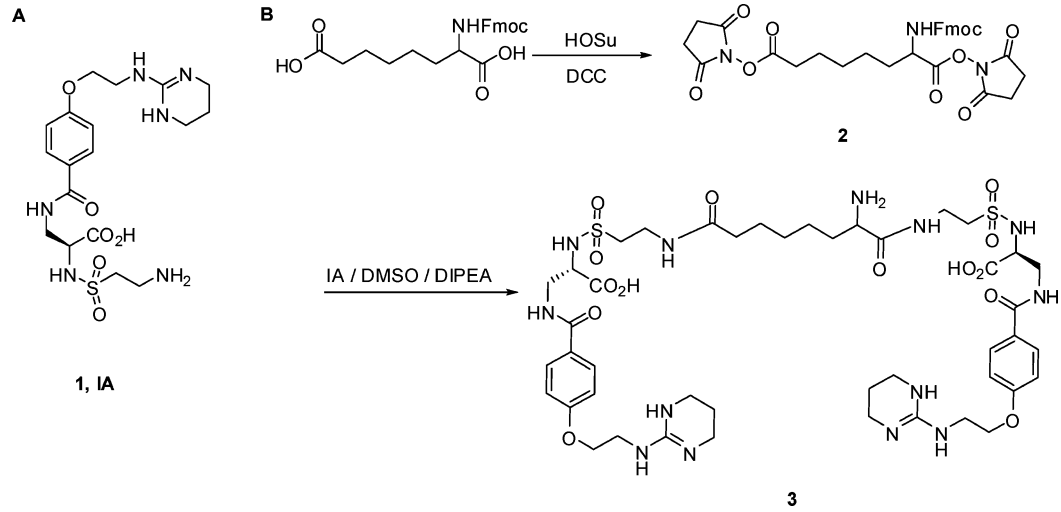

Figure 1. Schematic structure of IA **1** (A); synthetic scheme of bivalent IA **3** (B).

mance liquid chromatography (HPLC) system equipped with a diode array UV−vis absorbance detector (Agilent 1200 HPLC system). Mass spectral data were recorded on a ThermoFinnigan LCQ Fleet using electrospray as the ionization method. U-87 glioblastoma cells were obtained from American Type Culture Collection and were grown in Dulbecco's Modified Eagle's Medium DMEM (DMEM) supplemented with 10% fetal bovine serum (FBS) at 37 °C in humidified atmosphere.

Computer Modeling. The *AutoDock* program (version 3.0.5) was used for docking calculations (*12*). The graphical program *SYBYL* (version 16.91, Tripos, Inc.) was used for model building of the ligand structures, to generate missing hydrogen atoms and assign partial charges for protein targets used in AutoDock runs, and for energy minimization of initial ligand structures. Structural figures were generated using *WebLab Pro*.

Protein Coordinates. The structure of extracellular segment of integrin $\alpha_v\beta_3$ (PDB entry 1jv2) was used for the docking simulations of integrin $\alpha_v\beta_3$. The extracellular segment of the human integrin structure contains two subunits α (957 residues) and β (692 residues). The $\alpha_v\beta_3$ when complexed with Arg-Gly-Asp (RGD) reveals that the pentagonal peptide inserts into a crevice between the propeller and βA domains on the integrin head (*4*). The RGD sequence makes the main contact area with the integrin, and each residue participates extensively in the interaction, which is completely buried in the protein interior. For our simulations, we selected subunit β, and used Glu^{220}, Asn^{215}, Asp^{217}, and Pro^{219} as the target coordinate for binding, as they are in close contact with RGD. No water molecules were included. Sybyl was used to add essential hydrogens and assign partial charges from the Kollman united-atom force field to the target protein.

Ligand Coordinates. The structures of bivalent-IA-Cy5.5 were built in SYBYL Biopolymer package and energy minimized with MMFF94 force field by 100 steps. The orientations of ligands were overlaid on the integrin $\alpha_v\beta_3$ in the crystal structure to allow similar starting coordinates to be used. Prior to docking runs, all ligand structures were translated arbitrarily 30 Å from the surface of the $\alpha_v\beta_3$. Because the ligands are highly flexible, with multiple rotatable dihedrals present even in the monvalent system, we adopted a two-stage strategy for protein/ligand complex structure modeling, involving simulated annealing (SA) and rigid docking, that partially takes into account ligand flexibility. In the SA step, a 1 ns MD trajectory was generated for each ligand at a temperature of 1500 K. Structures saved every 1 ps underwent energy minimization, and the optimized structures were sorted by energy. Our long-term goal is to use 5−10 lowest-energy structures of the ligand, thus identified, in rigid docking to the integrin. In our preliminary studies, we only employed a single conformer for each ligand—the lowest-energy structure from the SA run. At this stage, the conformational analysis was approximate, as a crude solvation model was employed, with interactions with solvent described by introducing a distance-dependent dielectric constant.

Simulation of Substrate Binding Using AutoDock. The auxiliary program AutoGrid was used for generation of affinity grid fields. The program assigned the center of the grids automatically. The dimensions of the grid were 60.0 Å × 60.0 Å × 60.0 Å with grid points separated by 0.375 Å. The ligands were then docked using the Lamarckian Genetic Algorithm (LGA). The parameters for the LGA configurational search were identical for all docking jobs. Ligand flexibility was taken into account by including rotations around bivalent-IA-Cy5.5 single bonds in the conformational search. The maximum translation step was kept constant at 0.2 Å for every cycle, but the maximum quaternion rotation step and dihedral rotation step had a reduction factor of 0.99 per cycle starting from a maximum rotation of 5.0°. For the search to be extensive, the program uses a multiple starting approach in combination with a time-dependent random number generator. The number of runs was set to 10. For each run, a population of 50 individuals was used, with at most 250 000 function evaluations used and run for at most 27 000 generations. The first top individual was preserved each generation. The mutation rate was 0.02 and the crossover rate 0.80. The GA's selection window was 10 generations; the α parameter was set to 0. After docking simulations had been carried out, the 10 solutions produced were grouped into clusters such that the ligand rms deviations within each cluster were below 0.5 Å. The clusters were also ranked by the value of the lowest-energy solution within each cluster. The lowest-energy solution and the solutions with energies within 5 kcal/mol of this value were considered as possible binding models.

Bivalent Ligands Synthesis. Bivalent ligand 3 was synthesized in three steps (Figure 1). To a solution of the 2-(((9*H*-fluoren-9-yl)methoxy) carbonylamino) octanedioic acid (100 mg, 0.24 mmol) in EtOAc (20 mL), dicyclohexylcarbodiimide (110 mg, 0.53 mmol), and *N*-hydroxysuccinimide (60 mg, 0.52 mmol) were added at 0 °C. The mixture was stirred at 0 °C for 8 h (detected by TLC). Solvent was evaporated under reduced pressure to get the crude intermediate **2**. Compound **2** was dissolved in DMSO (9 mL) for next step reaction without further purification. To this DMSO solution, IA (250 mg, 0.50 mmol) and diisopropylethylamine (0.2 mL, 1 mmol) were added and the mixture was stirred at ambient temperature for 24 h. After

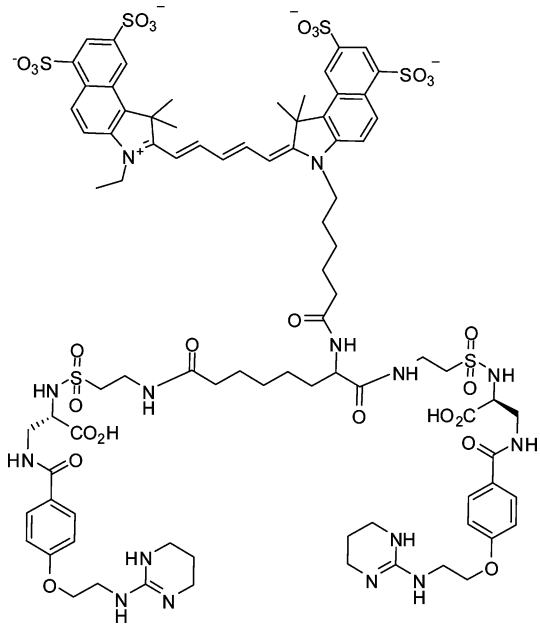

Figure 2. Schematic structure of bivalent-IA-Cy5.5 conjugate.

removing solvent at reduced pressure, 10 mL of water was added, and the white solid was removed by filtration. The aq solution was lyophilized, and the residue was recrystallized in methanol and acetone (1:3) to give pure bivalent IA **3** with 50% yield as white solid. ^{1}H NMR (300 MHz, D_2O): 7.65 (m, 4H), 6.93 (m, 4H), 4.16 (m, 7H), 3.84 (m, 4H), 3.30 (m, 10H), 3.21 (m, 10H), 2.05 (t, 2H, J = 7.0 Hz), 1.80 (m, 6H), 1.43 (m, 2H), 1.18 (m, 4H). MS (electrospray): m/z 1066.3 (100, $[M+H]^+$, calculated 1065.4); 533.8 ($[M+2H]^{2+}$. calculated 533.7).

Bivalent-IA-Cy5.5 Conjugate Synthesis. (Figure 2) Bivalent IA **3** (1.5 mg, 1.4 μmol) and 1.2 equiv of Cy5.5-NHS (2.0 mg, 1.7 μmol) were dissolved in 1 mL DMSO, and then 0.1 mL triethylamine was added. The reaction mixture was stirred in the dark at ambient temperature overnight and then quenched by adding 200 μL of 5% acetic acid (HOAc). The crude product was purified by a semipreparative reversed-phase HPLC employing a PhenomenexLuna C-18 column (250 mm × 10 mm) with the mobile phase starting from 95% solvent A (0.05% ammonia acetate in water) and 5% solvent B (acetonitrile) to 40% solvent A and 60% solvent B at 30 min, and the flow rate is 4 mL/min. Fractions containing bivalent-IA-Cy5.5 conjugates were collected, lyophilized, redissolved in saline at a concentration of 1 mg/mL, and stored in the dark at −20 °C until use. The analytical HPLC method was performed with the same gradient system, but with a Phenomenex C-18 column (250 mm × 4.6 mm) and flow rate of 1 mL/min. The purity of Cy5.5-labeled bivalent IA was over 98% from analytical HPLC analysis. The yield of bivalent-IA-Cy5.5 conjugate was over 70%. The purified bivalent-IA-Cy5.5 conjugate was characterized by mass spectroscopy (MS). MS (electrospray): m/z 1965.7 ($[M+H]^+$, calculated 1965.2); 983.1 (100, $[M+2H]^{2+}$, calculated 983.6). The absorption and fluorescence emission characteristics of bivalent IA-Cy5.5 conjugates were identical to those of free Cy5.5, as apparent from the spectra measured in H_2O (data not shown).

U-87 MG Xenograft Model. Animal procedures were performed according to a protocol approved by The Methodist Hospital Research Institute Animal Care and Use Committee (IACUC). Female athymic nude mice (nu/nu), obtained from Charles River Laboratories, Inc. (Cambridge, MA) at 4−6 weeks of age, were injected subcutaneously in the right rear thigh with 1×10^7 U-87 MG cells (see general procedures) suspended in 100 μL of phosphate-buffered saline (PBS). The cancer cells were harvested from subconfluent cultures with 0.25% trypsin. Trypsinization was stopped with DMEM containing 10% FBS, after which the cells were washed once in serum-free medium and resuspended in PBS. Trypan blue exclusion was performed to ensure >90% cell viability. The tumor bearing mice were subjected to *in vivo* imaging studies when the tumors reached 0.4−0.6 cm in diameter.

***In Vitro* Binding Assay.** To determine the receptor-binding ability, the bivalent ligands were tested for their ability to competitively inhibit the attachment of the natural ligand vitronectin to purified human $\alpha_v\beta_3$ by enzyme-linked immunosorbent assay (ELISA). Purified integrin $\alpha_v\beta_3$ protein (Chemicon International, Temecula, CA) was applied to 96-well polystyrene microtiter plates at 0.1 μg/well. After overnight incubation at 4 °C, the plates were washed and then blocked with milk solution (KPL, Inc., Gaithersburg, MD) at room temperature for 2 h. The blocking buffer was removed, and the plates were inoculated in quadruplicate with bivalent IAs with a typical starting concentration of 125 nM. Serial dilutions were prepared in the 96-well plates using multichannel pipettes. Biotinylated vitronectin solution (0.1 μg/well) was added to each well as a standard competitor. The plates were incubated at room temperature for 3 h, washed, and the bound vitronectin detected using NeutrAvidin-HRP conjugate at 0.01 μg/well (Pierce, Rockford, IL) and LumiGlo chemiluminescent substrate system (KPL, Inc., Gaithersburg, MD). The luminescence was read using a FLUOstar OPTIMA Microplate Reader (Durham, NC). The concentration of inhibitor producing 50% inhibition (IC_{50}) of vitronectin binding to $\alpha_v\beta_3$ was calculated on the basis of a curve fitting model using *KaleidaGraph 3.5* (Synergy Software, Reading, PA). c-[RGDfV] (Peptides International, Inc.) was also tested using the same method described above.

Fluorescence Microscopic Studies. To demonstrate that the bivalent-IA-Cy5.5 imaging probe can act as a specific ligand for $\alpha_v\beta_3$ integrin receptor in living cells, and to demonstrate the binding and subcellular localization of the bivalent probe, U-87 MG (ATCC HTB-14), a human glioblastoma cell line known to overexpress integrin $\alpha_v\beta_3$, was used in a probe binding assay (*4*). For fluorescence microscopy studies, 1×10^4 U87 cells were cultured on 35 mm MatTek glass-bottomed culture dishes. After 24 h, cells were washed with PBS and then incubated with bivalent-IA-Cy5.5 (200 nM) at 37 °C for 45 min. Integrin specificity of the probe binding was verified by incubating U87 cells with and without a blocking dose of the nonfluorescent bivalent IA (20 μmol/L). After the incubation period, the cells were washed three times with ice-cold PBS. The fluorescence signal of the cells was recorded using FluoView 1000 laser scanning confocal microscope (Olympus) under a 40× oil immersion objective, with laser excition at 675 nm (Cy5.5). A differential interference contrast image was also taken so that the origin of fluorescent signals could be confirmed.

***In Vivo* Fluorescence Imaging of Tumors.** ~3×10^6 U-87 cells were implanted bilaterally in the posterior flanks of immunocompromised (nu/nu) mice and grown to ~4−6 mm in diameter. Imaging was carried out with a group of 5 mice. After palpable masses were detected, animals were manually restrained and imaging probes were intravenously administered (lateral tail vein) using a 30 G needle via aseptic technique. Free Cy5.5 was prepared by dissolving the same Cy5.5NHS ester used for labeling the bivalent IA (GE Healthcare) in phosphate buffered saline (PBS), pH 7.4, overnight at 4 °C. Stock concentration of free Cy5.5 was measured optically using the molar exctinction coefficient of 250 000 M^{-1} cm^{-1} using a UV−visible spectrophotometer using the maximum absorbance wavelength (675 nm) as recommended by the supplier (GE Healthcare). The bivalent-IA-Cy5.5 was weighed and confirmed

Table 1. Conformational Energy of Bivalent IA and NIR Imaging Probe

Form of IA	Linker composition	Linker Length	Conformational Energy (kcal/mol)
Monomer	N/A	N/A	-17.0 ± 2.0
Dimer (IA-X-IA)	$(-C-)_n$	n = 1	-37.0 ± 2.0
		n = 2	-50.0 ± 2.0
X = linkers		n = 3	-53.0 ± 2.0
		n = 4	-49.0 ± 2.0
		n = 5	-60.0 ± 2.0
Near Infrared (NIR) (IA-X-P-IA) X = linker; P =probe molecule	(-C-)n	n =5	-53.0 ± 2.0

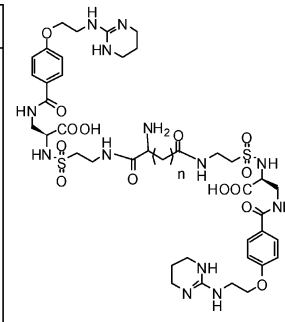

IA dimer

by spectrophotometer measurements. Appropriate dilutions of each probe were made in PBS, pH 7.4, and filter sterilized (0.2 μm) immediately prior to use. All animals weighing between 18 and 20 g received 10 nmol of imaging probe (total volume of 100 uL). Fluorescence imaging was performed with a small animal dedicated optical imaging system (Xenogen/Caliper IVIS-200, Mountain View, CA) under continuous 1.5−2.0% isoflurane delivered through the integrated anesthesia system. At 2, 4, 7, 24, and 48 h postinjection, images were acquired with the surface of the tissue of interest (tumor) approximating a perpendicular viewing angle relative to the camera line of sight; this viewing angle was also used for normal tissue selection. For determining tumor contrast, mean fluorescence intensities of the tumor area (*T*) defined as radiance (photons/s/cm^2/sr) at the right rear leg of the animal and of the area (*N*) at the right flank (normal tissue) were calculated by region-of-interest (ROI) analysis using the corresponding photograph of each image acquisition data set to identify the tumor region. Preinjection imaging was also performed to determine baseline autofluorescence. For competitive inhibition studies, mice (n = 3) were coinjected with 500 nmol bivalent IA and 10 nmol of imaging probe (bivalent-IA-Cy5.5) following the same procedure described above. Free Cy5.5 studies were performed in the same manner following the intravenous injection of 10 nmol. For ex vivo biodistribution imaging, two tumor-bearing mice were imaged 24 h post injection of bivalent-IA-Cy5.5 and thereafter euthanized per IACUC protocol (CO_2 and cervical dislocation). Tumor and major internal organs (heart, lung, liver, spleen, gastrointestinal tract, and kidneys) were harvested, weighed, and imaged against a black paper background. All image acquisition parameters were as follows: epi-illumination; Cy5.5 Em/Ex; Bin: (HR)4, FOV: 12.9; f2; 0.2 s.

Data Processing and Statistics. All data are given as means ± SD of n independent measurements. Statistical significance was assigned for P values less than the boundaries of tumors. Quantitative data were acquired with the software provided from the instrument's manufacturer (*Living Image*, v 3.1). Statistics software from R Development Core Team (2009). (R: A language and environment for statistical computing. R Foundation for Statistical Computing, Vienna, Austria. ISBN 3-900051-07-0, URL http://www.R-project.org).

RESULTS

Computer Modeling. From calculations of binding energies and ligand spatial distributions, the prediction of favored protein−ligand binding modes, interaction strengths, and binding specificity can be obtained with AutoDock simulations. Ten (10) LGA (Lamarckian genetic algorithm) docking runs were performed for each protein−ligand pair, with each run producing one possible binding mode or solution. The solutions were first sorted in terms of the binding mode, i.e., the position and orientation of the ligand relative to the protein target. The solutions were clustered on the basis of rms (root-mean-square) deviations in ligand atomic positions, with structures with rmsd of less than 0.5 Å grouped into a cluster. The total number of generated low-energy clusters measures the specificity of binding (*12–15*). A small number of clusters indicates that the ligand has only a few possible binding modes and interacts with a specific site (or sites) on the target protein. On the other hand, a large number of clusters implies existence of a wide range of binding modes and lack of specific ligand−target interactions. The second step in sorting solutions involves identification of the solution of lowest binding energy within each cluster and ranking the different clusters according to this energy value. The solution with the lowest energy in the top-ranked cluster and all solutions with energies higher by up to 5.0 kcal/mol were considered as possible binding modes for ligand to target.

Docking of Bivalent-IA-Cy5.5 to the Integrin $\alpha_v\beta_3$. A summary of the AutoDock results is presented in Table 1; the docked structures of the first and second clusters are shown in Figure 3. The docking of bivalent-IA-Cy5.5 to the integrin $\alpha_v\beta_3$ produced 3 clusters out of 10 runs. There were 5 solutions in the first cluster with an average docking energy of −34.04 kcal/mol. The binding site defined by this cluster is in the cleft between the RGD binding domain in integrin $\alpha_v\beta_3$. It is observed that bivalent-IA-Cy5.5 stays at that site in the presence of the whole protein. This cluster presents the best model for a possible bivalent-IA-Cy5.5 interaction to the integrin $\alpha_v\beta_3$. A comparison of the AutoDock results suggests that this binding conformation corresponding to the linker length of the bivalent-IA-Cy5.5 is a better substrate of integrin $\alpha_v\beta_3$. The binding of bivalent-IA-

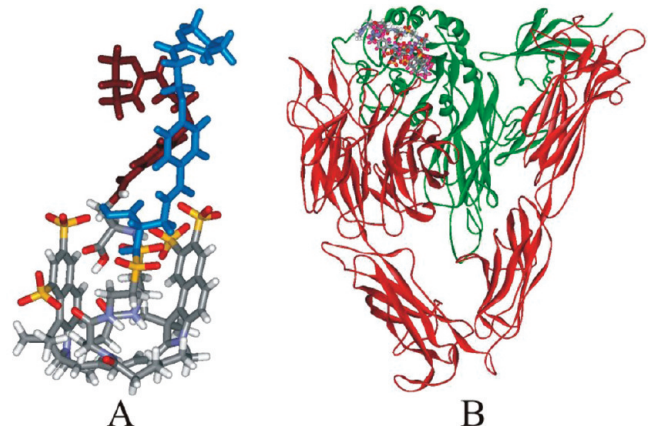

Figure 3. The lowest-energy conformation of bivalent-IA-Cy5.5 conjugate (A). Interaction of bivalent-IA-Cy5.5 with the Integrin (B). The lowest energy conformation is obtained from the analysis of molecular dynamics trajectories. Integrin structure is obtained from the open form of integrin crystal structure (1JV2).

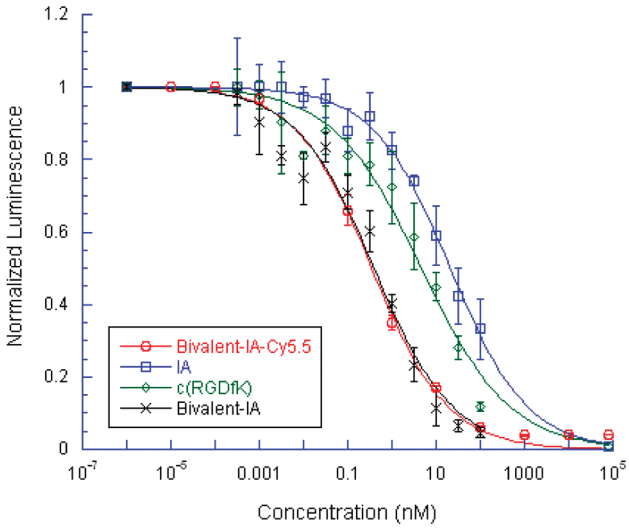

Figure 4. Enzyme-linked immunosorbent assay (ELISA) of IA (IC_{50}: 22.33 ± 4.51 nM), bivalent IA (IC_{50}: 0.40 ± 0.11 nM), bivalent-IA-Cy5.5 conjugate (IC_{50}: 0.13 ± 0.02 nM), and c-[RGDfV] (IC_{50}: 4.80 ± 3.01 nM). All of the points were done in triplicate.

Cy5.5 to the protein is stronger (lower energy) and more specific (small number of clusters) compared to other conformations with different linker length. The microscopic reason for these effects appears to be a lack of fit between different Cy5.5 conformation and the inhibitor/substrate binding site. The docking results are approximate. The scoring is based on an empirical energy function, solvation effects treated with a highly simplified model, and only ligand flexibility taken into account, with the protein structure kept fixed (*12–15*). Thus, the AutoDock results should only be considered as qualitative. The calculated binding energy results are in qualitative agreement with the observed inhibitory effects. Additionally, the simulations suggest that bivalent-IA-Cy5.5 with this conformation has a higher specificity and better fit into the known active site than other conformations.

***In Vitro* Binding Affinity.** Enzyme-linked immunosorbent assay (ELISA) was used to measure the competitive binding of antagonists and biotinylated human vitronectin for the immobilized integrin $\alpha_v\beta_3$. The IC_{50} value for parent compound IA, bivalent IA, bivalent-IA-Cy5.5 conjugate, and c-[RGDfV] were 22.33 ± 4.51, 0.40 ± 0.11, 0.13 ± 0.02, and 4.80 ± 3.01 nM, respectively (Figure 4). Cy5.5 conjugation did not decrease the receptor binding affinity of the resulting NIR fluorescent bivalent IA.

Fluorescence Microscopy. Bivalent-IA-Cy5.5 conjugate was incubated with U87 cells known to overexpress integrin $\alpha_v\beta_3$. Images were taken with a confocal fluorescent microscope. Receptor-mediated endocytosis was observed in the cells. The binding of bivalent-IA-Cy5.5 to U87 cells was effectively blocked by coincubation with nonfluorescent bivalent IA (Figure 5).

***In Vivo* Imaging of Integrin Overexpression in Xenograft U-87 Tumors.** Whole animal fluorescence imaging of subcutaneously implanted U-87 xenograft tumors demonstrated increased signal in tumor sites at 7, 24, and 48 h postconstrast injection (Figure 6). Imaging at earlier time points (2 and 4 h) showed intense systemic fluorescence signal due to relatively slow clearance of the compound. However, at 7 h, there is sufficiently high tumor-to-normal tissue (*T*/*N*) contrast to clearly discern the lesion; and by 24 and 48 h, the most intense signal is evident at the tumor site. Region of interest (ROI) analysis was performed by determining the boundaries of superficial tumors based on photographic images; this region was then measured for fluorescence signal (radiance units, photons/s/cm^2/steradian). Normal tissue was selected by copying the ROI of each sample to a site in the anterior flank. As plotted in Figure 7, *T*/*N* ratios reach a plateau at 24 h with an average maximum of ∼1.84. For the 7, 24, and 48 h time points, the fluorescence signals of the tumor and normal tissues were statistically significantly different (two sample, one side *t* test, *p*-value 0.006, 0.015, and 0.007, respectively, $n = 5$).

To ascertain the specificity of this tumor tissue signal localization, competitive inhibition studies were carried out using the nonfluorescent (without Cy5.5) bivalent IA. Using the same tumor model, a 10-fold excess of bivalent IA was coadministered with 10 nmol of bivalent-IA-Cy5.5 and were imaged at

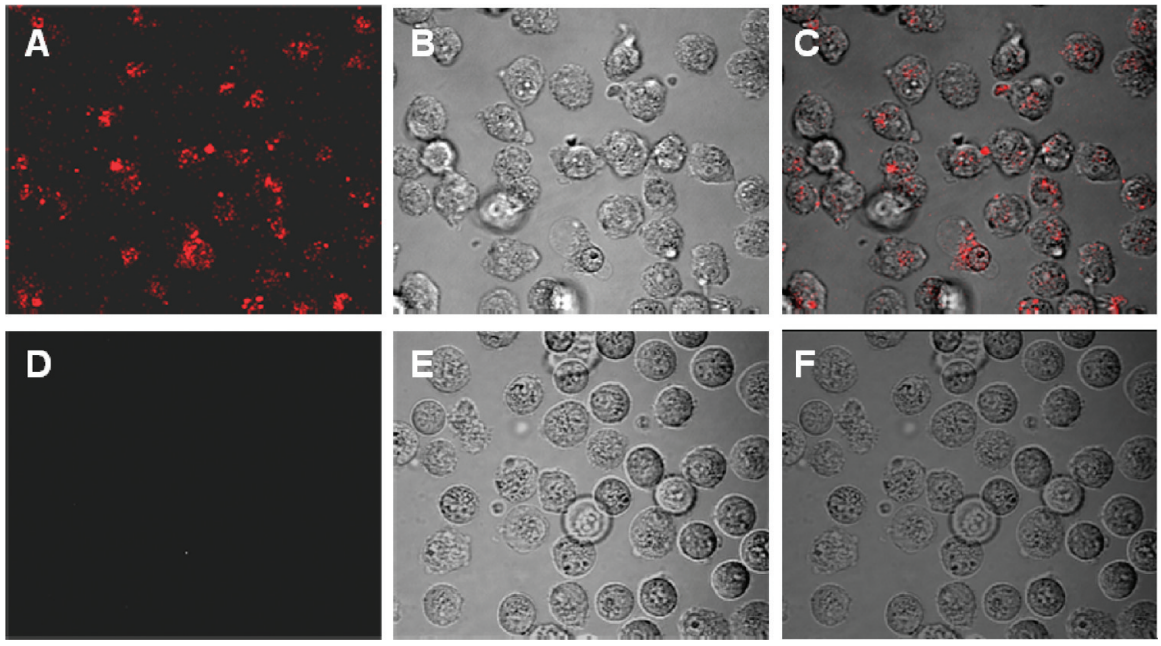

Figure 5. Specific binding of the bivalent-IA-Cy5.5 with U-87 cells. The left (A,D), middle (B,E), and right panels (C,F) represent fluorescence, brighten, and fusion images, respectively, taken from the same field of view. Confocal laser-scanning microscopy images of U-87 glioblastoma incubated with bivalent-IA-Cy5.5 demonstrated endocytosis of the imaging probes (A−C). U-87 cells blocking experiment with nonfluorescent bivalent IA demonstrated a complete blockage of endocytosis of the imaging probes (D−F).

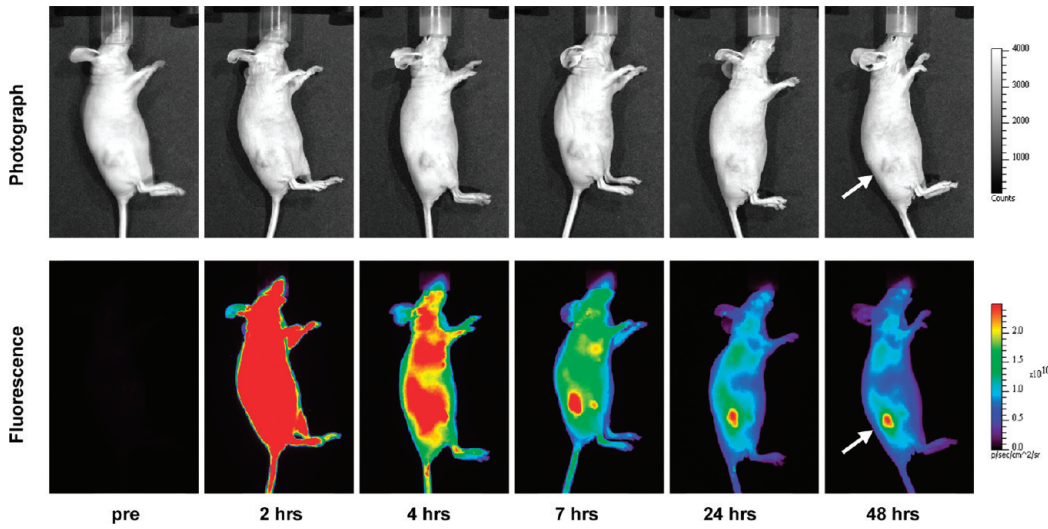

Figure 6. In vivo fluorescence imaging of live U-87 xenograft tumor-bearing mice. Photograph images (top panel) of representative mouse subject at selected time points. Photon scale is shown in the right; corresponding near-infrared fluorescence imaging (bottom panel). Radiance scale is shown in the color bar to the right (p/s/cm^2/sr). Subject was anesthetized with 1.5−2.0% isoflurane through a nose-cone. Arrow indicates tumor.

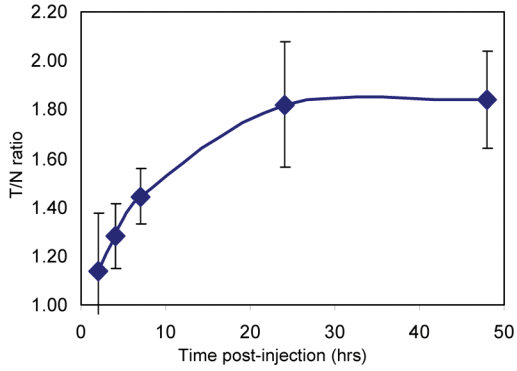

Figure 7. Region of interest (ROI) analysis of fluorescence signal (radiance) from tumor relative to normal tissue (*T*/*N*) vs time course following bivalent-IA-Cy5.5 administration (in hours). Error bars at each time point represents standard deviation from $n = 5$ subjects.

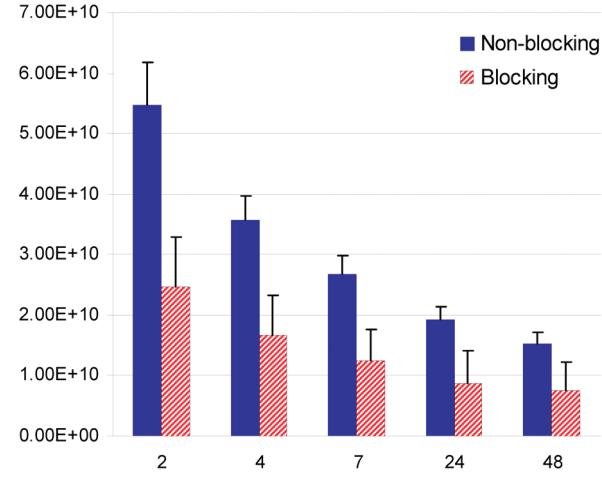

Figure 8. Competitive inhibition of bivalent-IA-Cy5.5 conjugate with nonfluorescent bivalent IA. Significant blocking of tumor fluorescence signal (*y*-axis) was observed at all time points (*x*-axis). Units of radiance (p/s/cm^2/sr). Error bars indicate SD from SD ($n = 6$ blocked, $n = 4$ nonblocked).

2, 4, 7, 24, and 48 h. ROI analysis was again performed as described above. When compared between blocking and nonblocking controls, fluorescence signals within tumors were reduced at all time points measured but were most pronounced in the earlier time points (2, 4, and 7 h), perhaps due to differing clearance rates of the two compounds (Figure 8). Nonetheless, the observed blocking effect was significant at all time points (two samples, one side *t* test, $p = 0.001$ (2 h); 0.002 (4 h); 0.003 (7 h); 0.012 (24 h); and 0.019 (48 h); $n = 6$ (blocking); $n = 4$ (nonblocking control). As a negative control, two tumor-bearing animals were intravenously injected with 10 nmol of the free Cy5.5 and imaged at 24 h post-injection. As shown in Figure 9, there is an overall reduction in systemic fluorescence signal from the entire animal. The relative amount of fluorescence signal from the tumor appears to be slightly higher than the background but is lower than that achieved with the bivalent-IA-Cy5.5 (Figure 9, compare left and right panels). This result is best explained by a higher clearance rate of the free fluorophore and a certain degree of nonspecific binding to tumors as observed by other investigators (*16*). Collectively, these data support the specificity of the bivalent-IA-Cy5.5 for integrin $\alpha_v\beta_3$ associated with U-87 tumors.

Given the intrinsic limitation in tissue penetration of excitation and emission photons from fluorophores, ex vivo imaging was performed to assess the fluorescence signal of the tumor relative to internal organs. Following the intravenous administration of the bivalent-IA-Cy5.5, two tumor-bearing animals were imaged as described above, imaged at 24 h postinjection and immediately thereafter euthanized for harvest of internal organs. Tumors and the major organs—heart/lung (en bloc), liver, spleen, gastrointestinal tract, and bilateral kidneys—were resected and placed on a black background and imaged under the same imaging acquisition protocol (Figure 10). Quantitative analysis was performed by measuring the total photon flux of each selected tissue and divided by the mass (Figure 11). The highest signal per mass of tissue was observed for the tumor, followed next by the heart and lung (en bloc), and kidneys. These data indicate that the bivalent-IA-Cy5.5 is specific for the tumor tissue, likely through binding to its cognate integrin receptor. Given the moderate level of fluorescence signal in the heart and lung, this compound is likely to have a relatively slow blood pool clearance rate. Fluorescence signal from the kidneys suggests mainly renal clearance of the agent, and minimal liver signal suggest low hepatic metabolism. Detailed bio-

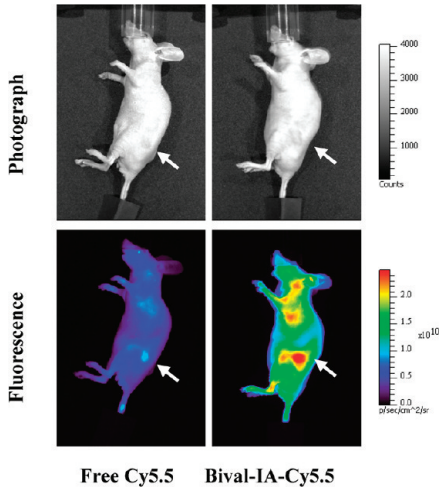

Figure 9. *In vivo* fluorescence imaging of live U-87 xenograft tumor-bearing mice at 24 h postintravenously administered unconjugated Cy5.5 (left panel) vs bivalent IA-Cy5.5 (right panel). Photograph images (top panel) of representative mouse subject. Photon scale is shown in the right; corresponding near-infrared fluorescence imaging (bottom panel). Radiance scale is shown in the color bar to the right (p/s/cm^2/sr). Mice were anesthetized with 1.5−2.0% isoflurane through a nose-cone. Black paper was used to cover the injection sites in the lateral tail veins. Arrows indicates tumors.

distribution, pharmacokinetic, and toxicity studies will be reported separately.

DISCUSSION

Glioblastoma multiforme (GBM) is the most common primary brain tumor, as well as the deadliest (*17*). Malignant gliomas present some of the greatest challenges in the management of cancer patients worldwide, despite notable recent achievements in oncology. Even with aggressive surgical resections using state-of-the-art preoperative and intraoperative neuroimaging, along with recent advances in radiotherapy and chemotherapy, the prognosis for GBM patients remains dismal. Mean survival after diagnosis is about 1 year (*18*). Preclinical data indicate that angiogenesis is essential for the proliferation and survival of malignant glioma cells, which suggests that inhibition of angiogenesis might be an effective therapeutic strategy.

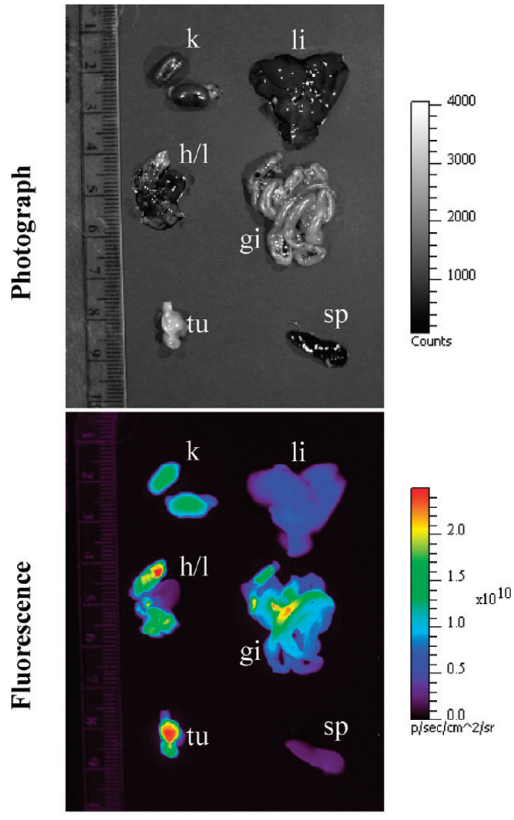

Figure 10. Representative *ex vivo* NIR imaging of major internal organs harvested from a xenograft tumor-bearing mice at 24 h post i.v. injection of bivalent IA-Cy5.5. Top panel: photograph (photon scale is shown to the right). Bottom: fluorescence image (p/s/cm^2/sr). Harvested organs are as follows: (k) kidneys; (li) liver; (h/l) heart and lungs; (gi) small and large intestines; (t) U-87 tumor; (sp) spleen.

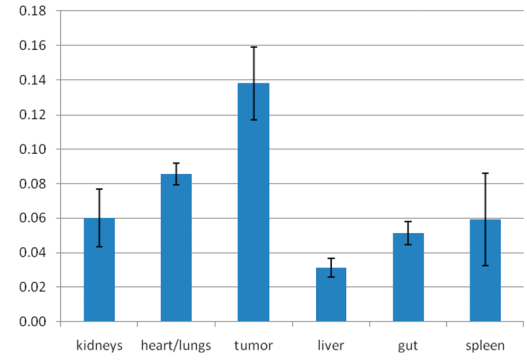

Figure 11. Biodistribution of bivalent IA-Cy5.5 at 24 h post-injection averaged from 2 subjects. *Y*-axis is total photon flux per gram of tissue.

NIRF imaging has been proven to be a very powerful tool for noninvasive imaging of various diseases in preclinical models especially in rodents (*10*). In an effort to leverage this robust modality, we sought to apply NIRF imaging techniques for studying an important molecular target, integrin $\alpha_v\beta_3$, expressed by glioblastoma cells. Our ultimate goal was to develop imaging and therapeutic agents targeted to integrin $\alpha_v\beta_3$ for early detection, treatment, and monitoring of glioblastoma as well as other malignancies. To achieve this goal, we set out to design and develop a highly specific and sensitive NIRF agent for this clinically important target.

Computer-assisted approaches to identify new inhibitors via pharmacophore, molecular modeling, docking, and structural interaction fingerprints is rapidly becoming an integral part of rational approaches to drug design. In silico assessment of the free energy and the binding affinity of receptor-inhibitors prior to synthesis permits sophisticated and efficient methods to design drugs. Hood et al. demonstrated that the integrin antagonist, 4-[2-(3,4,5,6-tetrahydropyrimidine-2-lamino)ethyloxy]benzoyl-2-(*S*)-aminoethylsulfonyl-amino-*h*-alanine (IA) can be used as a targeting agent for gene delivery to tumor neovasculature (*2*). A rationally designed bivalent IA by computer modeling could theoretically have better binding affinity and thus greater avidly to target cells expressing this receptor. In an effort to develop the bivalent IA probe for tumor angiogenesis imaging, an extensive simulation with varying linker lengths and composition was carried out. Our results (shown in Table 1) demonstrated that bivalent IAs with linkers containing 5 to 8 carbons (n = 2−5) exhibited descending conformational energy, while the linker shorter than 5 carbons (n < 2) had a significantly higher energy. On the basis of these simulation results, we chose the 8-carbon linker (n = 5), which has the lowest conformational energy to construct the first bivalent IA. Among various commercially available linkers, 2-aminododecanedioic acid, which carries two carboxylic acid groups at each end with a total of eight carbons (n = 5), was chosen as the best linker for the prototype construct. This analysis predicted that the bivalent IA with an 8-carbon linker (n = 5) containing the NIR fluorophore, Cy5.5 dye, would not sterically impact the binding to the integrin protein.

In vitro binding assays have shown that the bivalent IA (IC_{50} = 0.40 ± 0.11 nM) exhibited significantly improved integrin $\alpha_v\beta_3$ affinity when compared to the parent compound IA (IC_{50} = 22.33 ± 4.51 nM), resulting in a 50-fold improvement in receptor affinity (IC_{50}) over that of the parent compound IA and a 10-fold improvement over c-[RGDfV] (IC_{50} = 4.80 ± 3.01 nM). NIR imaging probe, bivalent-IA-Cy5.5 conjugate, also demonstrated significantly increased binding affinity (IC_{50} = 0.13 ± 0.02 nM). Fluorescence microscopy studies demonstrated integrin-mediated endocytosis of the bivalent-IA-Cy5.5 conjugate in U-87 cells, which was effectively blocked by nonfluorescent bivalent IA. This result provides strong supporting evidence that bivalent-IA-Cy5.5 binds specifically to the $\alpha_v\beta_3$ integrin receptor expressed on the tumor cell surface.

Systemically administered bivalent-IA-Cy5.5 in tumor-bearing mice resulted in modest accumulation at the tumor site with improved tumor/normal tissue signal over time (up to 48 h). This effect is best explained by the relatively slow clearance of the probe from the circulation as evident from the high fluorescence observed throughout the test animals at earlier time points (up to 24 h). Consistent with prior studies using a monomeric integrin peptidomimetic conjugated to a chelate for radioisotope imaging, tumor accumulation was time-dependent and required washout from normal tissue for optimal contrast (*8*). Although the tissue penetration of excitation and emission photons of near-infrared light is superior to wavelengths of the visible spectrum, a substantial percentage of light is attenuated as a function of tissue depth. Hence, fluorescence measurements likely underestimate the true accumulation of integrin-specific probes at the target tissue.

The experimental results presented here demonstrate the ability to noninvasively image integrin $\alpha_v\beta_3$ overexpression in live whole animals using a bivalent small molecule with improved receptor binding properties generated by in silico design. A major impetus for our experimental design was to demonstrate proof of concept in generating a new class of targeted imaging agents by leveraging known structure activity relationships and in silico modeling to further improve receptor binding properties of existing molecules. Prior multivalency studies have clearly shown the utility of expanding the repertoire of drugs by reconfiguring molecules as multimers (*19, 20*). We propose that such approaches will have significant impact in the drug discovery process by providing a mechanism to alter the pharmacologic properties of existing as well as novel drugs.

CONCLUSION

We have successfully synthesized and evaluated a novel near-infrared fluorescent nonpeptidic bivalent integrin $\alpha_v\beta_3$ antagonist for tumor imaging with improved binding avidity relative to the monovalent ligand. The design of this bivalent compound was facilitated by in silico modeling which guided synthetic strategy in a practical application of optimizing a biologically relevant imaging probe. We suggest that this approach represents a general paradigm to improve receptor binding affinities of extant compounds through rationally designed multivalent configurations. More research will be carried out to rationally design bivalent ligands with different types of linkers using computer modeling followed by *in vitro* and *in vivo* evaluation.

ACKNOWLEDGMENT

This work was supported by The Methodist Hospital Research Institute, the M.D. Anderson Foundation, and the Vivian L. Smith Foundation. GSJ would like to acknowledge support from Baylor Supercomputing Center and internal funding. We appreciate Dr. Shi Ke for discussion and advice on biological study.

LITERATURE CITED

(1) Brooks, P. C., Clark, R. A., and Cheresh, D. A. (1994) Requirement of vascular integrin alpha v beta 3 for angiogenesis. *Science 264*, 569–71.

(2) Hood, J. D., Bednarski, M., Frausto, R., Guccione, S., Reisfeld, R. A., Xiang, R., and Cheresh, D. A. (2002) Tumor regression by targeted gene delivery to the neovasculature. *Science 296*, 2404–7.

(3) Takagi, J., and Springer, T. A. (2002) Integrin activation and structural rearrangement. *Immunol. Rev. 186*, 141–63.

(4) Delbaldo, C., Raymond, E., Vera, K., Hammershaimb, L., Kaucic, K., Lozahic, S., Marty, M., and Faivre, S. (2008) Phase I and pharmacokinetic study of etaracizumab (Abegrin), a humanized monoclonal antibody against alphavbeta3 integrin receptor, in patients with advanced solid tumors. *Invest. New Drugs 26*, 35–43.

(5) Schottelius, M., Laufer, B., Kessler, H., and Wester, H. J. (2009) Ligands for mapping $\alpha_v\beta_3$-integrin expression in vivo. *Acc Chem Res 42*, 969–80.

(6) Chen, X., Conti, P. S., and Moats, R. A. (2004) In vivo near-infrared fluorescence imaging of integrin alphavbeta3 in brain tumor xenografts. *Cancer Res. 64*, 8009–14.

(7) Cheng, Z., Wu, Y., Xiong, Z., Gambhir, S. S., and Chen, X. (2005) Near-infrared fluorescent RGD peptides for optical imaging of integrin alphavbeta3 expression in living mice. *Bioconjugate Chem. 16*, 1433–41.

(8) Burnett, C. A., Xie, J., Quijano, J., Shen, Z., Hunter, F., Bur, M., Li, K. C., and Danthi, S. N. (2005) Synthesis, in vitro, and in vivo characterization of an integrin alpha(v)beta(3)-targeted molecular probe for optical imaging of tumor. *Bioorg. Med. Chem. 13*, 3763–71.

(9) Xie, J., Shen, Z., Li, K. C., and Danthi, N. (2007) Tumor angiogenic endothelial cell targeting by a novel integrin-targeted nanoparticle. *Int. J. Nanomed. 2*, 479–85.

(10) Ntziachristos, V., Bremer, C., and Weissleder, R. (2003) Fluorescence imaging with near-infrared light: new technological advances that enable in vivo molecular imaging. *Eur. Radiol. 13*, 195–208.

(11) Sevick-Muraca, E. M., Houston, J. P., and Gurfinkel, M. (2002) Fluorescence-enhanced, near infrared diagnostic imaging with contrast agents. *Curr. Opin. Chem. Biol. 6*, 642–50.

(12) Morris, G. M., Goodsell, D. S., Halliday, R. S., Huey, R., Hart, W. E., Belew, R. K., and Olson, A. J. (1998) Automated docking using a Lamarckian genetic algorithm and empirical binding free energy function. *J. Comput. Chem. 19*, 1639–1662.

(13) Goodsell, D. S., and Olson, A. J. (1990) Automated docking of substrates to proteins by simulated annealing. *Proteins 8*, 195–202.

(14) Morris, G. M., Goodsell, D. S., Huey, R., and Olson, A. J. (1996) Distributed automated docking of flexible ligands to proteins: parallel applications of AutoDock 2.4. *J. Comput. Aided Mol. Des. 10*, 293–304.

(15) Xiong, J. P., Stehle, T., Zhang, R., Joachimiak, A., Frech, M., Goodman, S. L., and Arnaout, M. A. (2002) Crystal structure of the extracellular segment of integrin alpha Vbeta3 in complex with an Arg-Gly-Asp ligand. *Science 296*, 151–5.

(16) Cheng, Z., Levi, J., Xiong, Z., Gheysens, O., Keren, S., Chen, X., and Gambhir, S. S. (2006) Near-infrared fluorescent deoxyglucose analogue for tumor optical imaging in cell culture and living mice. *Bioconjugate Chem. 17*, 662–9.

(17) Parsons, D. W., Jones, S., Zhang, X., Lin, J. C., Leary, R. J., Angenendt, P., Mankoo, P., Carter, H., Siu, I. M., Gallia, G. L., Olivi, A., McLendon, R., Rasheed, B. A., Keir, S., Nikolskaya, T., Nikolsky, Y., Busam, D. A., Tekleab, H., Diaz, L. A., Jr., Hartigan, J., Smith, D. R., Strausberg, R. L., Marie, S. K., Shinjo,

S. M., Yan, H., Riggins, G. J., Bigner, D. D., Karchin, R., Papadopoulos, N., Parmigiani, G., Vogelstein, B., Velculescu, V. E., and Kinzler, K. W. (2008) An integrated genomic analysis of human glioblastoma multiforme. *Science 321*, 1807–12.

(18) Kanu, O. O., Mehta, A., Di, C., Lin, N., Bortoff, K., Bigner, D. D., Yan, H., and Adamson, D. C. (2009) Glioblastoma multiforme: a review of therapeutic targets. *Expert Opin. Ther. Targets 13*, 701–18.

(19) Rao, J., Lahiri, J., Isaacs, L., Weis, R. M., and Whitesides, G. M. (1998) A trivalent system from vancomycin.D-ala-D-Ala with higher affinity than avidin.biotin. *Science 280*, 708–11.

(20) Mulder, A., Huskens, J., and Reinhoudt, D. N. (2004) Multivalency in supramolecular chemistry and nanofabrication. *Org. Biomol. Chem. 2*, 3409–24.

BC900313D